

## Article

# A Resistivity Plate Loading Device for Assessing the Factors Affecting the Stiffness of a Cement-Stabilized Subgrade

Huaiping Feng<sup>1</sup>, Ackah Frank Siaw<sup>2,\*</sup>  and Hailiang Wang<sup>1</sup>

<sup>1</sup> State Key Laboratory of Mechanical Behavior and System Safety of Traffic Engineering Structures, Shijiazhuang Tiedao University, Shijiazhuang 050043, China; fenghuaiping@stdu.edu.cn (H.F.); wanghailiang@gmail.com (H.W.)

<sup>2</sup> Key Laboratory of Mechanical Behavior Evolution and Control of Traffic Engineering Structures in Hebei, Shijiazhuang Tiedao University, Shijiazhuang 050043, China

\* Correspondence: frank@stdu.edu.cn; Tel.: +86-156-1414-0411

**Abstract:** The extent of mixing in the stabilization process and the control of the cement content ( $C$ ) and water content ( $w$ ) in the mixture are key to the outcome of the engineering performance of a cement-stabilized subgrade. Intelligent Compaction (IC) quality control has improved quality control and management practices during construction. Intelligent Compaction Measurement Values (ICMVs) selected to evaluate the stiffness properties of cement-stabilized soils do not directly relate to the stiffness properties of the cement-stabilized subgrade and do not consider  $w$  and  $C$ . Additional tests need to be conducted for calibration of ICMVs. In this study, our solution is the development of a resistivity plate loading test. The resistivity plate loading test features the flexibility in determining the soil stiffness,  $w$ ,  $C$ , and other important factors, such as the time of test effect (hydration) ( $T$ ) and dry density ( $\rho_d$ ). To verify the accuracy of the testing method, laboratory experimental studies were conducted on cemented soils considering  $\rho_d$ ,  $w$ ,  $C$ , and  $T$  at different factor levels. Multiple response studies based on grey rational analysis (GRA) were conducted. Analysis of the input factors was performed, and their effects on the measured responses were quantified. According to the study, the  $\rho$  measured by the device was a powerful indicator of stiffness,  $\rho_d$ ,  $w$ ,  $C$ , and  $T$ , which showed that the device can be useful equipment for quality control and an advancement in the in situ testing technologies and test equipment. A statistical regression model based on the linear and linear plus interaction terms among the factors is proposed to predict the average responses.

**Keywords:** resistivity plate loading test; water content; cement hydration; subgrade reaction modulus



**Citation:** Feng, H.; Siaw, A.F.; Wang, H. A Resistivity Plate Loading Device for Assessing the Factors Affecting the Stiffness of a Cement-Stabilized Subgrade. *Materials* **2022**, *15*, 3453. <https://doi.org/10.3390/ma15103453>

Academic Editors: Cesare Oliviero Rossi, Pietro Calandra, Paolino Caputo, Bagdat Teltayev, Valeria Loise and Michele Porto

Received: 16 February 2022

Accepted: 7 May 2022

Published: 11 May 2022

**Publisher's Note:** MDPI stays neutral with regard to jurisdictional claims in published maps and institutional affiliations.



**Copyright:** © 2022 by the authors. Licensee MDPI, Basel, Switzerland. This article is an open access article distributed under the terms and conditions of the Creative Commons Attribution (CC BY) license (<https://creativecommons.org/licenses/by/4.0/>).

## 1. Introduction

Soil stabilization with cement is a well-established practice for constructing rail/roadway embankments and pavement layers. Cement stabilization allows the improvement of both standard soils and substandard in situ soils to levels consistent with the construction requirements. The stiffness and performance of stabilized subgrades are related to how close the stabilized subgrade is to achieving optimal compaction properties. As a result, standard test methods, fundamental analysis, design procedures, and quality evaluation are available to obtain acceptable results [1–5]. However, significant challenges still exist for the accurate quality assessment of compacted soil properties under in situ conditions.

Current in situ quality evaluation testing techniques include stiffness test methods [6–13]. Stiffness spot test methods are less frequently employed, as the number of test points is limited, certain test methods are time-consuming, and they cause interference with the construction operations. Intelligent compaction (IC) quality control that integrates a vibratory roller with an accelerometer-based measuring system, a high-precision global positioning system (GPS), and an on-board data acquisition system to monitor the compaction process is highly recommended [8,10]. IC quality control overcomes the limitations of traditional stiffness spot test methods. Studies suggest that stiffness spot test methods

must be conducted to calibrate intelligent compaction measurement values (ICMVs). The calibration makes IC achieve 100% coverage for various subgrade soils utilized for construction, with benefits such as improved compaction, uniformity, reduced over/under compaction, and the ability to identify weak spots, as well as design, construction, and performance integration. However, stiffness spot test methods and IC do not detect the  $w$  and  $C$ , which significantly affect cement-stabilized subgrades [14–16].

Studies and experience show that  $w$ ,  $C$ , and  $\rho_d$  can vary based on the construction method. The quality control process may sometimes be delayed because of anticipated problems, such as the organization of the crew to the site or faulty equipment [17,18]. The hydration reaction between  $w$  and  $C$  causes the stiffness,  $w$ , and  $\rho_d$  to change with  $T$ . As a result, it is essential to clarify the correct  $C$ ,  $w$ ,  $\rho_d$ , and  $T$ . This finding ensures an accurate assessment of the stiffness properties to predict the improvement effects of the stabilized subgrade [3,19–21]. Below/above the optimum  $w$  and  $C$  requirements, the required engineering properties may not reach/exceed the design limit, which may produce different physical and stiffness characteristics of the stabilized subgrade [22]. It is purportedly reported that some of these characteristics might be unfavorable to certain dynamic and traffic-loading conditions, thus affecting the pavement life and performance [11,23–28]. Therefore, gaining insight into the relationship between these properties requires improved/new test methods that are capable of concurrently and instantaneously assessing the stiffness and physical properties.

Recently, integrated geophysical mechanical test methods have been employed to solve many geotechnical problems [29–31]. The most common integrated geophysical test method is soil resistivity ( $\rho$ ). The  $\rho$  of compacted cement-stabilized soils depends on factors such as  $w$ ,  $\rho_d$ , porosity, and temperature [32,33]. The  $\rho$  of the cement-stabilized soil is affected by the changes in the compaction.  $\rho$  is selected to measure and characterize soil properties during in situ and laboratory tests [29–31]. Models are available to describe the  $\rho$  of several geomaterials, including cement soil mixtures [32–34]. Thus,  $\rho$  can be an alternative indicator of the changes in the mechanical and physical properties of cement-stabilized soil. Incorporated  $\rho$  cone penetrometer [29], triaxial [30,35], and consolidation devices [31] have been used to evaluate the mechanical and physical properties of cement-stabilized subgrade, which produced excellent results. However, there is a lack of equipment and methodological approaches for simultaneously and non-destructively assessing the  $\rho$ , soil stiffness,  $w$ ,  $C$ , and  $\rho_d$  properties for in situ quality evaluation of cement-stabilized subgrade.

In this study, we aimed to develop and apply the resistivity plate loading test ( $\rho$ PLT) to assess the properties of compacted cement subgrade. We further assessed the effect of variations in  $\rho_d$ ,  $w$ ,  $C$ , and  $T$  on the stiffness of the cemented subgrade, adopting the Taguchi design of the experiment. Furthermore, mathematical relationships were developed to predict  $K_{30}$ ,  $\rho$ , the unconfined compression strength (UCS), and all the quality parameters by adopting grey rational analysis (GRA).

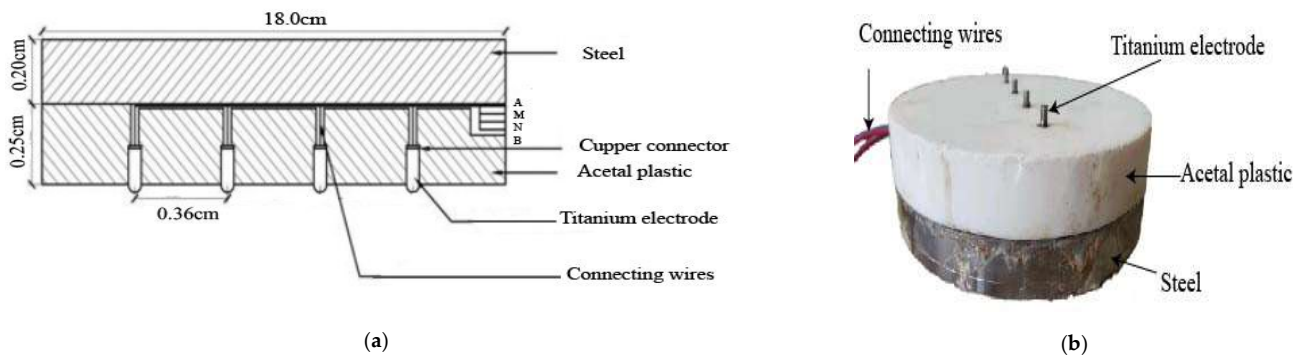
#### *Resistivity Plate Loading Device*

Figure 1a shows a section of a typical resistivity plate loading device and Figure 1b shows a picture of the device, which comprises mild steel, a resistivity metre, and titanium electrodes (diameter of 4.0 mm and height of 7.0 mm) properly insulated with acetate plastic. The Wenner four-probe method of  $\rho$  measurement was employed. This technique is commonly applied in geology and soil science  $\rho$  measurements. Aside from the Wenner configuration method, several other electrode configuration methods are available in the literature and are rich in theory. Refs. [36,37] discuss the merits and demerits of the various electrode configuration methods. The suitability of a particular array depends on the signal-to-noise ratio, depth of investigation, geometry of the electrode, etc. The Wenner four-probe electrode arrangement was chosen, and instrumental sensitivity was not as important as in the other array geometries. The electrode spacing determines the depth of electrical current penetration and volume measurement. In a homogeneous soil, the soil volume measured is approximately  $\pi a^3$ , where (a) is the electrode spacing. In an experiment, a resistivity meter

is connected to the loading plate, i.e., two electrodes (A and B) for injecting current into the stabilized subgrade and two voltage electrodes (M and N) for measuring the potential difference. Equation (1) is used to convert the current and voltage to an apparent resistivity.

$$\rho = K \frac{\Delta V}{I} \quad (1)$$

where  $K$  is the geometrical factor dependent on the electrode configuration; for the Wenner configuration,  $K = 2\pi a$ ,  $\pi$  is 3.14,  $a$  is the electrode space,  $V$  is the voltage, and  $I$  is the current.



**Figure 1.** Resistivity plate loading device. (a) A section of the laboratory resistivity loading plate and (b) a picture of the resistivity loading plate.

The  $\rho_{PLT}$  method can be used to assess a whole range of soils, including subgrade, subbase, base, and treated soils used for road and railway construction. A calibration procedure may be required to avoid errors in  $\rho$  measurements when  $\rho_{PLT}$  is conducted on soils in rocks [38]. The electrodes of the resistivity plate loading device may also suffer contact resistance problems when installed on frost, very dry soils, and soils in rock [38,39].

In an experimental setup,  $\rho$  measurement errors have two origins: (1) poor electrode contact and (2) instrumental noise. The electrode depth (7.00 mm) and diameter (4.00 mm) induce minor faults in the former. In the latter, measurement time causes minimal or no variation in the  $\rho$  measurement. The properties of the electrode geometry and configuration are similar to other laboratory measuring instruments available in the literature [40].

Acetal plastic has excellent mechanical and low moisture absorption properties. Additionally, the coefficient of friction of acetal is within the range of metals that are commonly employed for static loading plates. As a result, the acetal plastic may have minimal or no effect on the stiffness measured with this device.

## 2. Experimental Program, Materials, Soil Preparation, and Testing

### 2.1. Experimental Program

The experimental program involves (1) testing the basic properties of the soil, (2) determining the most significant factors that affect the compaction quality of the cement-stabilized subgrade and their factor levels, and (3) selecting an orthogonal array and running the experiments based on the orthogonal array. The experiments conducted included the unconfined compression strength (UCS) test and resistivity subgrade reaction modulus test ( $\rho K_{30}$ ).

### 2.2. Soil Properties

The soil used for this study was obtained from Hebei, China. The soil is classified as A-2-4 according to the American Association of State Highway and Transportation Official (AASHTO) and SP-SM according to the Unified Soil Classification System (USCS). Figure 2 shows the particle size distribution curve. The liquid limit is 29.52% and the plastic limit is 19.19%. The uniformity coefficient ( $C_u$ ) is 48.461, the coefficient of gradation ( $C_c$ ) is 0.57, and the group index (GI) is 0.

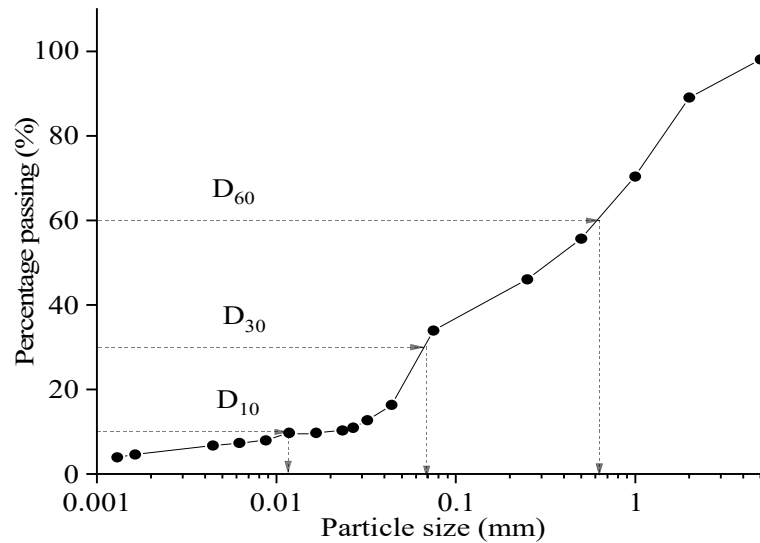


**Figure 2.** Particle size distribution curve.

ASTM D558-96 procedures were followed to determine compaction characteristics. The test results were applied to determine the maximum dry density (MDD) and optimum moisture content (OMC). The test was conducted by adding ordinary Portland cement of grade 32.5 to the soil in proportions of 5%, 8%, and 12% by weight of the total soil dry mass. The mixture was thoroughly mixed until uniformity was achieved. Figure 3 shows the compaction characteristics. Twelve percent C was considered to give the best results. Ref. [37] recommended adding 5–12% C to soils with similar properties.

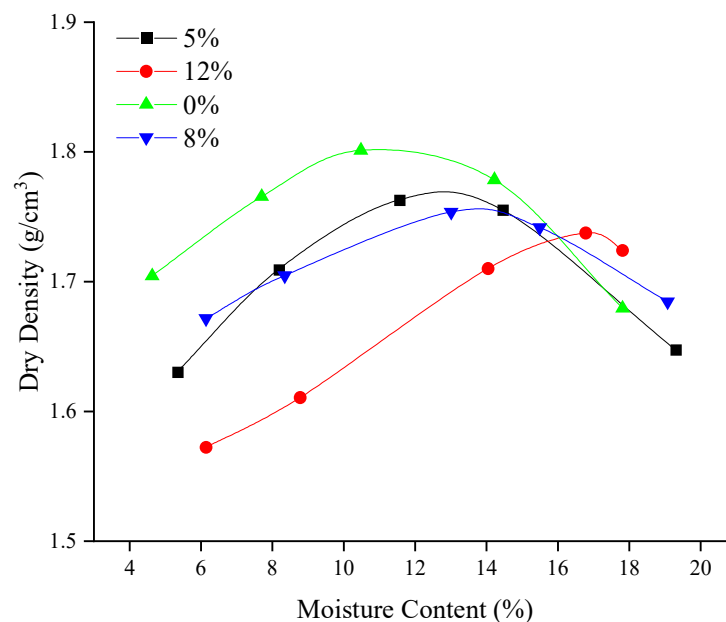


**Figure 3.** Compaction characteristic of the compacted soils.

### 2.3. Development of Taguchi Orthogonal Array

The  $\rho_d$ ,  $C$ ,  $w$ ,  $T$ , and other factors, such as the particle size and shape of the soil, type of cement, porosity, temperature, etc., affect the in situ strength and compaction quality control of the cement-stabilized subgrade [17,18,41]. The Taguchi method may be employed to assess the essential factors for compaction quality control and quality assurance. The Taguchi method works on the principles of an orthogonal array and provides fewer variances in results, with an optimal set of control parameters. The principle allows the characterization of complex behavior, maximizing the test coverage while

minimizing the test cases to be considered and the ease of data analysis [42,43]. Table 1 presents the factor levels, and Table 2 presents details of the Taguchi orthogonal array design used in this study. The control factors were carefully selected based on previous research [1,44,45].  $\rho_d$ ,  $w$ ,  $C$ , and  $T$  were selected as control input parameters, and their corresponding levels were determined as shown Table 1.

**Table 1.** Experimental factors and their levels.

Factor	Level 1	Level 2	Level 3
$\rho_d$	1.70 g cm <sup>-3</sup>	1.76 g cm <sup>-3</sup>	1.80 g cm <sup>-3</sup>
$w$	8%	12%	18%
$C$	5%	12%	18%
$T$	2	24	48

**Table 2.** Taguchi L9 Orthogonal array for conducting the design of experiments and test results.

ID	Taguchi Orthogonal Array				Test Results					
	$\rho_d$ (g·cm <sup>-3</sup> )	$w$ (%)	$C$ (%)	$T$ (h)	K30 (MPa/m <sup>2</sup> )		$\rho$ ( $\Omega$ m)		UCS (MPa)	
					Average	St.d	Average	St.d	Average	St.d
1	1.70	5.0	8.0	2.0	95.33	0.67	47.10	1.43	0.88	0.03
2	1.70	12.0	12.0	24.0	103.3	3.33	66.29	0.77	3.12	0.06
3	1.70	18.0	18.0	48.0	130.10	2.67	100.00	2.89	0.93	0.04
4	1.76	5.0	12.0	48.0	173.33	0.00	108.20	0.62	3.18	0.04
5	1.76	12.0	18.0	2.0	140.00	1.67	100.00	0.11	2.26	0.08
6	1.76	18.0	8.0	24.0	118.50	1.50	52.10	2.18	4.66	0.10
7	1.80	5.0	18.0	24.0	179.98	2.68	123.99	0.09	5.66	0.13
8	1.80	12.0	8.0	48.0	153.34	2.66	90.94	2.21	4.21	0.06
9	1.80	18.0	12.0	2.0	110.83	2.50	59.27	0.26	8.25	0.08

St.d is standard deviation.

The Taguchi method works best in processes and procedures where one quality characteristic is to be evaluated. However, many practical applications are a compendium of quality characteristics. Multicriteria decision-making methods are often utilized in such complex scenarios. Recommended multicriteria decision-making methods include grey relational analysis (GRA), techniques for order preferences by similarity to ideal solution (TOPSIS), the analytic hierarchy process (AHP), etc. More than one quality characteristic was assessed, turning the multiple responses into a single response problem. Multicriteria decision-making methods have been suggested to be useful, easy, and efficient when integrated with the Taguchi method [46], with the most common methodologies being GRA and TOPSIS with several modifications. The GRA method was employed in this study to combine all the multiple response values into a single response value; thus, an interrelationship between the responses based on the grey relational coefficient was obtained. The GRA method has the following advantages: the results depend on the original values of the measured responses; the calculations are simple and suitable for multiple complicated relationships between responses and fairness comparison; and dimensional attributes are ensured by normalization. The steps to employ the GRA technique are as follows:

Step 1. Define a set  $A$  of  $n$  alternatives concerning  $W$  evaluation criteria as follows

$$A = [b_{ij}]_{m+n} = \begin{bmatrix} b_{11} & b_{12} & \cdots & b_{1m} \\ b_{12} & b_{22} & \cdots & b_{2m} \\ \vdots & \vdots & \ddots & \vdots \\ b_{n1} & b_{n2} & \cdots & b_{nm} \end{bmatrix} \quad (i = 1, 2, \dots, n \text{ and } j = 1, 2, \dots, m) \quad (2)$$

where  $b_{ij}$  represents the response value of the  $i$ th alternative on the  $j$ th criterion.

Step 2. If the quality characteristic expectancy maximizes the response, use the larger, the better Equation (3). Use the smaller, the better Equation (4) when the quality characteristic minimizes the response. Use Equation (5) for nominal quality characteristics.

$$\bar{b}_{ij} = \frac{b_{ij} - \min(b_{ij}, i = 1, 2, \dots, n)}{\max(b_{ij}, i = 1, 2, \dots, n) - \min(b_{ij}, i = 1, 2, \dots, n)} \quad (3)$$

$$\bar{b}_{ij} = \frac{\text{Max}(b_{ij}, i = 1, 2, \dots, n)}{\max(b_{ij}, i = 1, 2, \dots, n) - \min(b_{ij}, i = 1, 2, \dots, n)} \quad (4)$$

$$\bar{b}_{ij} = \frac{(|b_{ij} - T|) - \min(|b_{ij} - T|), i = 1, 2, 3, \dots, n)}{\max(|b_{ij} - T|, i = 1, 2, \dots, n) - \min(|b_{ij} - T|, i = 1, 2, \dots, n)} \quad (5)$$

Step 3. Compute the grey relational coefficient (GC) for normalization using Equation (6).

$$GC_{ij} = \frac{\Delta_{\min} + \lambda \Delta_{\max}}{\Delta_{ij} + \lambda \Delta_{\max}} \quad (6)$$

Step 4. Compute the grey rational grade ( $G_i$ ) using Equation (7).

$$G_i = \frac{1}{m} \sum GC_{ij} \quad (7)$$

where  $m$  is the number response;  $\Delta_{\min}$  is minimum value of  $\Delta$ ;  $\Delta_{\max}$  is maximum value of  $\Delta$ ;  $\lambda$  is the distinguishing coefficient which is defined in the range  $0 \leq \lambda \leq 1$ , (in this study 0.5 was used);  $GC_{ij}$  is the gray relational coefficient for the  $i$ th experiment and  $j$ th response;  $T$  is the target value. In this study, average response was used.

#### 2.4. Soil Preparation

Large soil lumps were broken with a wooden mallet, oven-dried at a temperature of 105 °C, and allowed to cool. All calculations were based on the oven-dried soil mass. The required amount of soil and  $w$  were calculated, thoroughly mixed in a bowl, transferred into plastic bags, and then tightly sealed. The samples were then kept for a day for moisture equilibration. Afterwards, the required amount of C was calculated, added, and mechanically mixed until the clumps formed were less than 5% of the total mix.

Samples prepared for the model test were cast into the modified soil consolidation soil chamber unit and subjected to an impact compaction test. The weight of the material in the container was calculated. The mixture was compacted in three equal layers. In each layer, a temperature sensor that was properly insulated was installed to monitor the temperature evolution during the curing process. The temperature evolution has an important consequence on the strength development and  $\rho$  measurement [47,48]. The specimens were cured in an open dry place under sealed conditions. All samples were cast into a thin, insulated steel cylinder, and their upper surfaces were tightly sealed using a plastic cover.

Two (2) samples were prepared for the UCS test, adopting the sample plan in Table 2. The ASTM D 1633 (2014) standard requires samples with a diameter, height, and height-to-diameter ratio (h/d) of 101.60 mm, 116.40 mm, and 1.15, respectively, or samples with a diameter, height, and h/d ratio of 71.10, 142.20 mm, and 2.00, respectively. In this study, samples were prepared at a height of 80.00 mm and diameter of 39.10 mm with an h/d ratio of 2.05. The height and weight of the prepared samples were within an accuracy of  $\pm 1\%$ . The prepared samples were stored in a zip-lock polythene bag under damp conditions. The mixing, compaction process, and each test was completed in less than two (2) hours. The UCS was tested in a triaxial loading frame with a computerized data-acquisition system at a loading rate of 1.00 mm/min (ASTM D1633).

### 2.5. Test Setup

Figure 4c shows the details of the test setup, which comprises a loading system (air cylinder, air compressor, air pressure regulator, and air pressure gauge), deformation measurement system (linear variable displacement transducers (LVDTs)), computerized data-acquisition system,  $\rho$ PLT device, temperature sensors (embedded within the compacted soil; bottom, middle, and upper-lower with rubber on it), and a soil-containing unit (diameter of 25.20 cm; height of 27.00 cm).

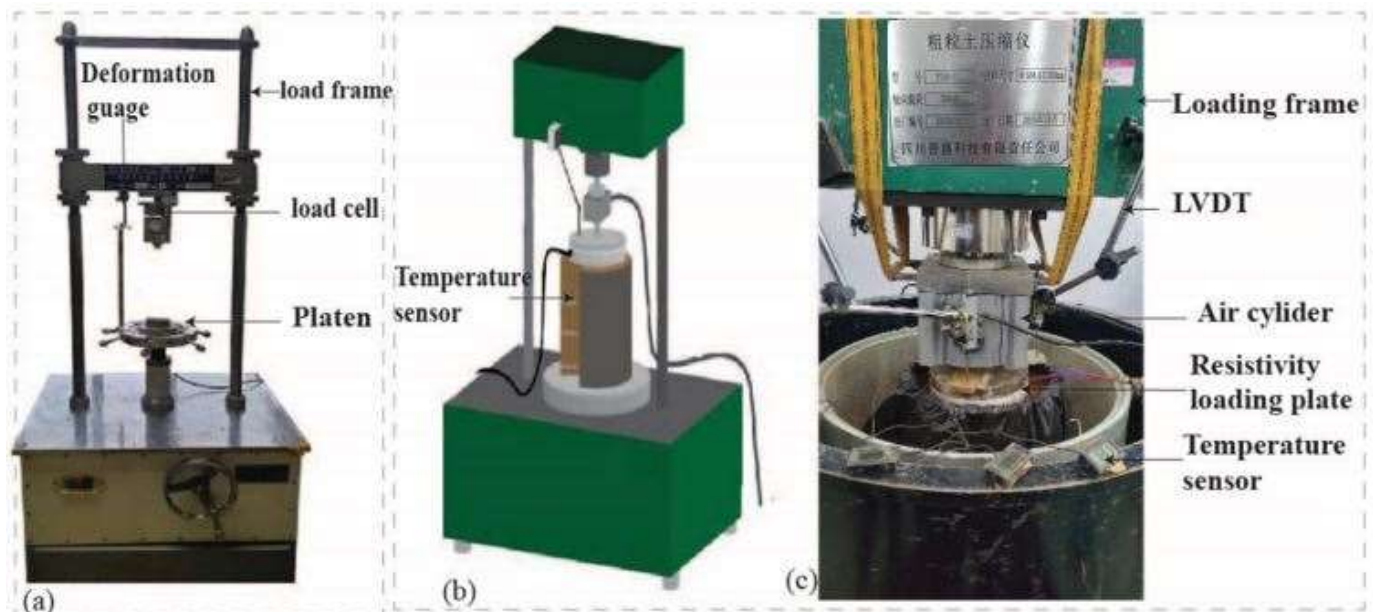


**Figure 4.** Experimental device. (a) UCS testing machine; (b) 3D drawing of the model test; (c) picture of the model test.

The temperature sensors utilized a Pro Led DC 12 V digital thermometer and sensor probes with a temperature range of  $-50$  to  $110$  °C.

The soil-containing unit was constructed of a steel frame with a height of 30.0 cm and a diameter of 25.2 cm. A plastic bag was inserted into the container, and the soil was packed into and compacted using the impact method. The plastic bag prevented the walls from conducting electrical current during testing. The walls of the soil container were also such that they exerted minimal or no effects on the stresses and strains during testing.

The soil-containing unit edges exert a border effect on the infinite value of the resistivity of air. These border effects are significant challenges for laboratory  $\rho$  measurements. Solutions have been developed in [49]. The  $\rho$  measured in our study is affected by this border effect. However, we do not intend to correct this measurement. The testing conditions are similar to those likely to be experienced for in situ conditions in a typical railway or a road embankment where the geometry may be a 2- or 3-dimensional structure surrounded by air. Accounting for these possible conditions will be complicated.

## 3. Testing Process

### 3.1. Temperature

The temperature sensors were monitored every fifteen minutes for the first two hours. Afterwards, the temperature sensors were read every two hours during the daytime until the curing periods ended.

### 3.2. Resistivity Subgrade Reaction Modulus Test

$\rho$ PLT was selected to assess the properties of the model samples. The subgrade reaction modulus ( $K_{30}$ ) test was conducted according to the procedures of TB10621-2014.

The required load was applied through the piston to the load plate from an air cylinder supported by a reaction frame. The air cylinder was regulated through the air regulator. When the required air was supplied to the air cylinder, the valve that opened to the air cylinder was closed until the next load application was opened. This step was repeated throughout the test. LVDTs with an accuracy of 0.01% of the full range (100 mm) were mounted on three (3) sides of the load plate and configured to a computer that automatically displayed the deformation readings. The average deformation reading was employed for all calculations. For accuracy, all the devices were calibrated after three (3) sample runs during testing. The equivalent  $K_{30}$  was calculated with Equation (8).

$$K_{30} = \frac{\sigma}{s_D} \quad (8)$$

where  $K_{30}$  is the equivalent subgrade reaction modulus,  $s_D = 1.25$  mm multiplied by  $(D/30$  cm);  $D$  is the diameter of the resistivity loading plate, and  $\sigma$  is the stress at  $s_D$ .

$\rho$  was measured with an ETCR3000B digital grounding resistance soil resistivity tester.  $\rho$  was recorded five minutes after every load application, which reduces the variability of  $\rho$ .

### 3.3. Unconfined Compression Strength Test

After curing the samples for 28 days, the samples were immersed in water for no less than four (4) h. Afterwards, the soil samples were removed from the water, dampened, and tested. During testing, loads were applied until the load at failure was recorded. The UCS strength was calculated using Equation (9). The ASTM D 1633 recommends multiplying the samples prepared with method B by 1.10 to obtain the calculated UCS strength. Based on laboratory studies, [50] suggested multiplying samples with an  $h/d$  ratio of 2.0 by a factor of 0.86. This step was purposely applied to convert the strength of an  $h/d$  ratio of 2.00 to that of the  $h/d$  ratio of 1.15, which is commonly utilized in routine soil-cement testing. In this study, a factor of 1.10 was applied.

$$q_u = \frac{P(1 - \epsilon)}{A_0} \times F \quad (9)$$

where  $q_u$  is the UCS strength;  $P$  is the force applied;  $\epsilon$  is axial strain;  $A_0$  is the cross-sectional area of the specimen; and  $F$  the strength correction factor.

### 3.4. Explanation of Test Results

#### 3.4.1. Compaction

The compaction characteristics of soils are evaluated regarding OMC and MDD. Figure 3 shows the compaction characteristics. The sample with 0% cement content exhibited the highest MDD compared with the other samples. The relatively low MDD of the samples with cement additives, particularly 12%, can be attributed to (1) the cement additive, which causes aggregation of the soil particles to occupy large spaces that change the effective particle size of the soil; (2) the absorption of the compaction energy by the hydration products of the sample (the OMC increases with the addition of  $C$  due to the increase in  $w$  required for cement hydration); and (3) the loss of moisture due to evaporation from heat generated during hydration [13,51].

#### 3.4.2. Temperature

Figure 5 shows the temperature–time plot history for the tested samples. The sample with the highest temperature exhibited a peak temperature of 13 °C (1) and a low temperature of 1.0 °C (3). An exothermic chemical reaction between cement and water occurs when they are blended. Temperature, relative humidity, type of cement, and  $C$  can affect the reaction. The relatively low temperature observed was caused by environmental factors [52]. High-temperature conditions enhance cement hydration and pozzolanic reactions in cement-stabilized soils, thus improving the strength properties. However, very high

curing temperatures (20–60 °C) have caused cement hydration products to be arranged randomly, thus producing large pores in soils (crossover effect) [48]. Elsewhere, lower temperature conditions have also been reported to contribute to poor strength development [53]. The different temperature gradients affect the strength development and  $\rho$  measurement [48].

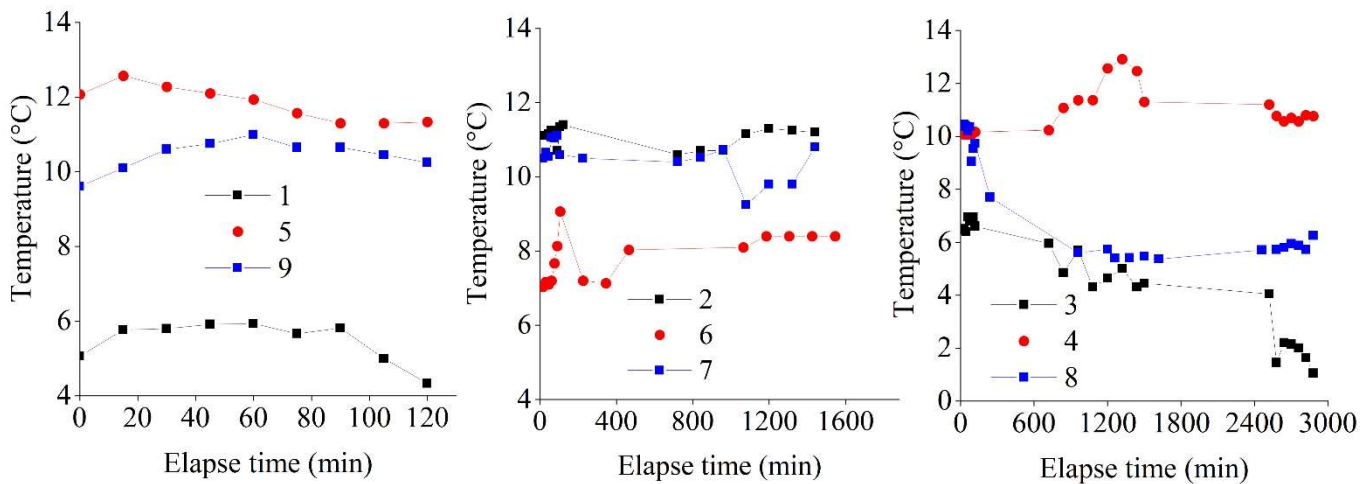


Figure 5. Temperature–time history plots for the tested samples.

### 3.4.3. Resistivity Subgrade Reaction Modulus

The study clearly showed the dependence of stiffness and  $\rho$  on  $\rho_d$ ,  $w$ ,  $C$ , and  $T$ . All  $\rho$  readings were temperature corrected using Equation (10). Figure 6a presents a typical stress- and temperature-corrected  $\rho$ , and the change in  $\rho$  with successive load application was a kind of multistage process during testing. We envisaged that the contacts between the electrodes and the soil would improve with successive loads acting on the loading plate. As forces were applied to the loading plate, comparable  $\rho$  changes were observed. The changes in  $\rho$  were analogous to the changes in the soil properties, interaction of the  $w$ , cement hydration products, and influence of the applied stress beneath the loading plate. For a given  $T$ , the higher the cement content is, the greater the number of hydration compounds, thus the higher the observed  $\rho$  [32]. Additionally, the lower  $w$  is, the higher the observed  $\rho$ . The selected  $\rho$  was calculated by establishing a linear equation between the measured  $\rho$  and the deformation.  $\rho$  is determined at the equivalent deformation used to calculate the subgrade reaction modulus. The test results are summarized in Table 2.

$$\rho_w(t) = \frac{\rho(t_0)}{1 + \alpha(t - t_0)} \quad (10)$$

where  $\alpha \approx 0.025$  ( $^{\circ}\text{C}^{-1}$ ),  $\rho_w(t)$  is the temperature-compensated electrical resistance,  $t_0$  is a fixed reference temperature, and  $\rho(t_0)$  is the  $\rho$  at a temperature  $t_0$ .

Figure 6a,b show the stress and resistivity curves and stress–strain curves for the tested samples. The samples exhibited different forms of stress and strain characteristics. Generally, strain hardening was observed for samples compacted at a higher  $w$  and low  $C$ . A similar observation was observed for certain samples with a low  $w$ . A linear elastic behavior was also observed for certain samples compacted at a higher  $\rho_d$ .

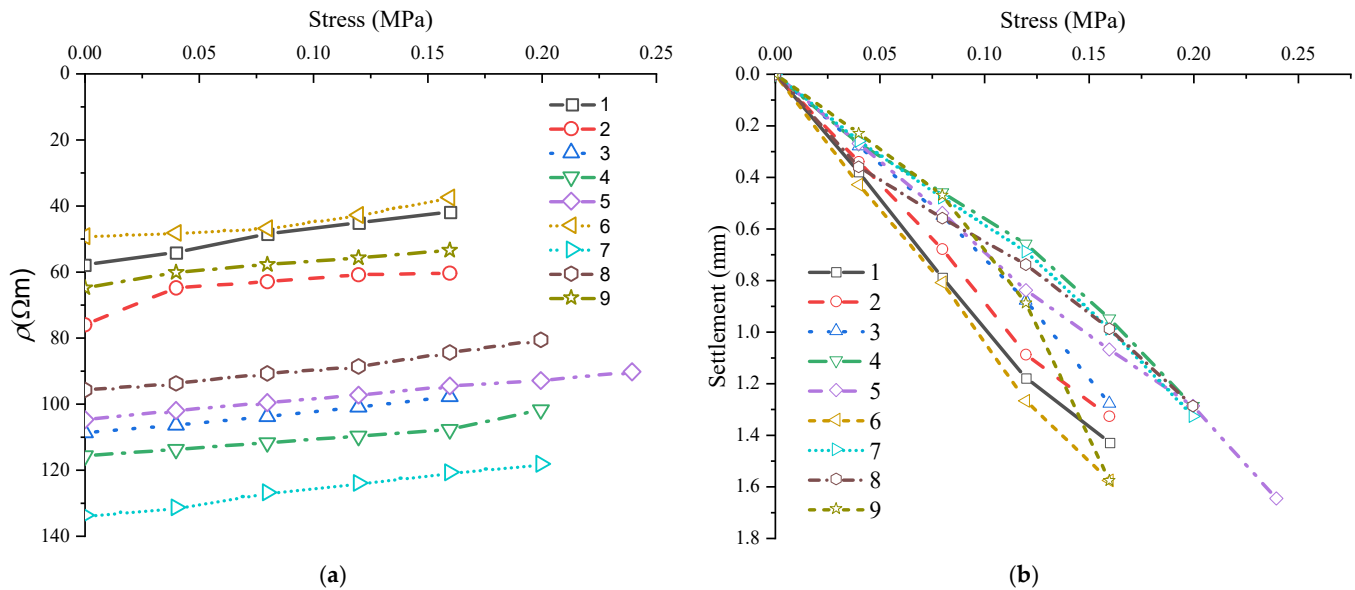


**Figure 6.** Resistivity plate loading test results (a) typical of stress- and temperature-corrected apparent resistivity curves from the concurrent resistivity subgrade reaction modulus test and (b) typical of the stress strain curves.

#### 3.4.4. Unconfined Compression Strength Test

The UCS is an index for quantifying the effectiveness of an additive [2,54] on the soil strength. The sample must not collapse, or no significant loss in strength should be observed during water immersion. The test results for UCS are presented in Table 2. The results range from 0.85 to 8.18. The highest results were associated with samples compacted at the highest  $\rho_d$ . The  $w$  and  $C$  content variation had a different effect on the UCS. UCS values in the range of 0.2–0.4 MPa are usually permitted for subgrade applications. However, considering the different compositions of the samples, they may have negative consequences on the performance of the compacted subgrade.

## 4. Discussion

### 4.1. Range Analysis

Range analysis was performed in the Minitab statistical package to assess the influence of the various factors on the response variables and their ranks, as shown in Table 3. The rank based on the Delta statistics compared the relative magnitudes of their effects. The delta statistic is the highest average minus the lowest average for each factor. The ranks and average level responses are used to determine which element provides the best results. All the means of the mean plots were determined using the nominal characteristics. Furthermore, all ANOVAs were performed at a confidence level of 95% and 5% significance level.

#### 4.1.1. Subgrade Reaction Modulus

In Table 3,  $\rho_d$ ,  $T$ ,  $w$ , and  $C$  are ranked in order of importance. The analysis of variance for the individual factor contributions and their  $F$  values of 1.74, 1.16, 0.67, and 0.62 are presented in the order of the ranks. As shown in Figure 7, a combination of 23  $\rho_d$ , 5%  $w$ , 18%  $C$ , and  $T$  of forty-eight (48) h is considered to give the best result. According to the literature, the strength of the cement-stabilized subgrade is related to the solid phase,  $w$ ,  $C$ , and  $T$  [19,55]. An increase in  $\rho_d$  yielded an increase in  $K_{30}$ , as shown in Figure 7. An increased  $\rho_d$  caused interlocking between the soil particles and cement particles, thus increasing the ability of the soil to resist the mechanical forces that act on it [56,57]. Additionally, an increase in  $w$  weakens the cohesion strength between the particles of the soil and the hydration products [18].

Table 3. Response table for mean.

Subgrade Reaction Modulus ( $K_{30}$ )				
Level	$\rho_d$	$w$	$C$	$T$
1	109.60	149.50	122.40	115.40
2	143.90	132.20	129.20	133.90
3	148.00	119.80	150.00	152.20
Delta	38.50	29.70	27.60	36.90
Rank	1.00	3.00	4.00	2.00
Soil electrical resistivity ( $\rho$ )				
1	71.27	93.25	63.52	69.12
2	86.78	80.31	72.69	75.36
3	91.59	70.64	108.00	99.72
Delta	20.32	22.60	44.48	30.61
Rank	4	3	1	2
Unconfined compression strength test (USC)				
1	1.64	2.87	3.25	
2	3.37	3.20	4.18	
3	5.01	3.95	2.58	
Delta	3.36	1.07	1.60	
Rank	1.00	3.00	2.00	
GRA				
1	0.82	0.55	0.57	0.61
2	0.52	0.67	0.64	0.62
3	0.42	0.53	0.54	0.52
Delta	0.40	0.14	0.09	0.11
Rank	1.00	2.00	4.00	3.00

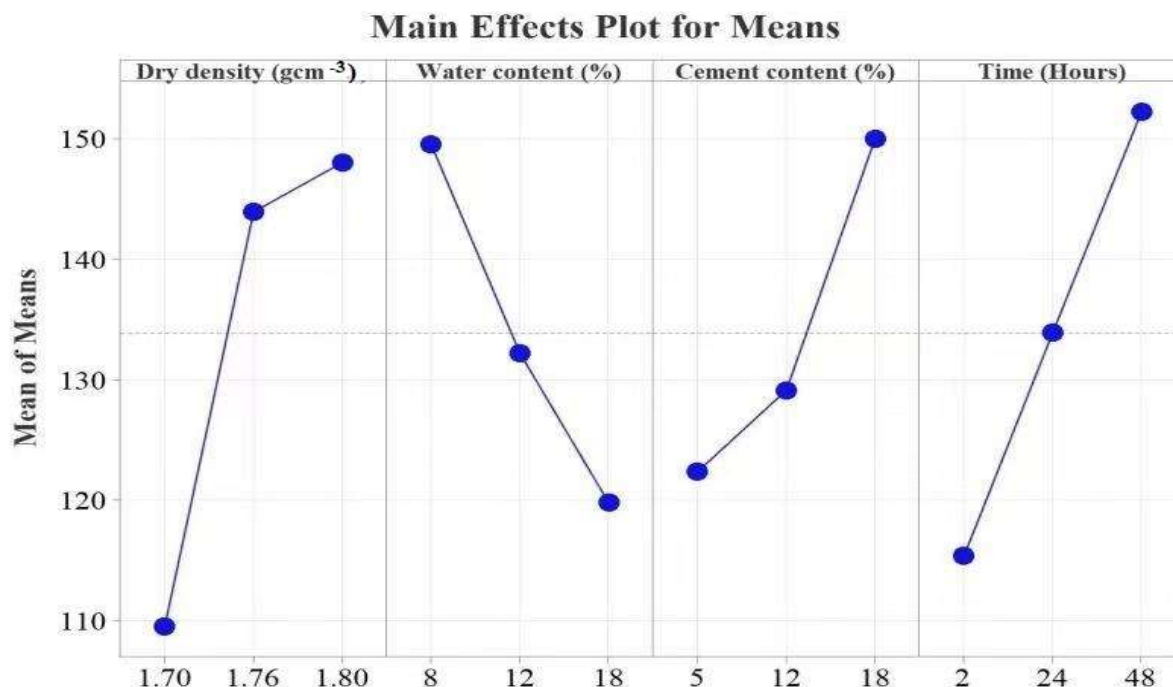
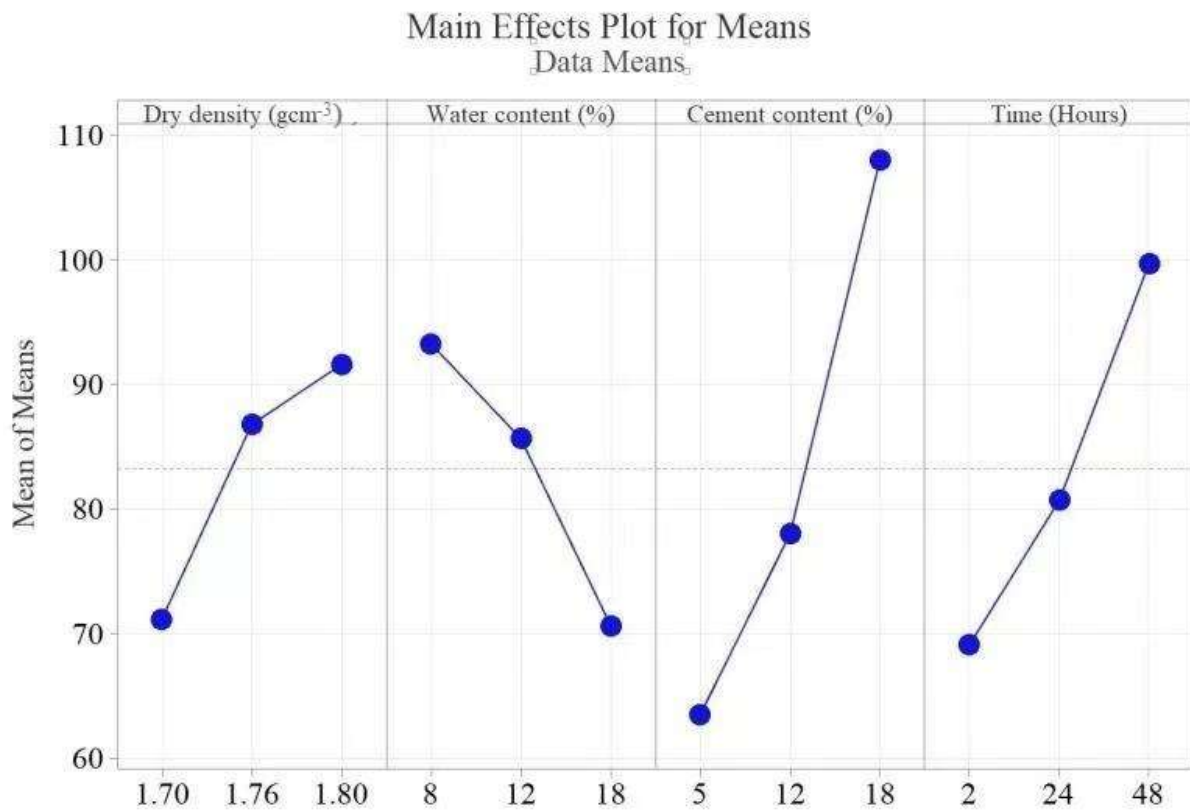


Figure 7. Effects of the control factors on the  $K_{30}$ .

#### 4.1.2. Resistivity

Table 3 shows the ranks of the input factors. The analysis of variance on the individual factor contributions and their F values according to the ranks ( $C$ ,  $T$ ,  $w$ , and  $\rho_d$ ) are 3.19, 0.94, 0.46, and 0.38, respectively.  $C$  exhibits a significant effect on the  $\rho$  response. As

shown in Figure 8, the line slope shows that the effect and the degree of the slope are comparative to the magnitude of the inputs.  $\rho$  increases with an increase in  $\rho_d$  and  $T$  and decreases with an increase in  $w$ . Several others have reported the same findings [32]. The  $C$  produces an amount of hydration products for a given  $T$ , resulting in a denser structure. The higher  $T$  is, the higher the hydration products produced. Thus, the free water space and porosity decrease and tortuosity increases, increasing  $\rho$ . Additionally, an increase in  $\rho_d$  causes interlocking and parking of the soil particles, which renders the electrical flow path tortuous, increasing  $\rho$ .



**Figure 8.** Effects of the control factors on the  $\rho$ .

#### 4.1.3. Unconfined Compressive Strength

Since all the samples were assessed at 28 days, the effect of curing was excluded. Subsequently,  $\rho_d$ ,  $w$ , and  $C$  were evaluated to determine their impact on the UCS strength development. Table 3 shows the ranks of the input factors. The F values of the input factors according to the ranks are 5.93, 0.54, and 0.23. Figure 9 presents the main effect plots. The best strength was achieved at 1.80  $\rho_d$ , 18%  $w$ , and 12%  $C$ . Several researchers using the UCS test have investigated the strength of cement-stabilized soil [44,58–60]. Almost all researchers reported an increase in strength with an increase in  $\rho_d$ , and our results confirm this finding. The UCS strength increases with an increase in  $\rho_d$  and  $w$  up to 12%  $C$ , as shown in Figure 9. At 18%  $C$ , the UCS decreases, which is contrary to the results presented in [44,53,58–62]. This observation can be explained by the observation that at higher  $C$ , the cement-treated soil requires enough  $w$  to undergo complete hydration [61,63]. Furthermore, at higher  $C$ , microcracks develop, easily propagating and joining under applied loads and thus reducing the UCS. This finding means that there is an optimum amount of  $w$  and  $C$  for which the number of bonds and their configuration offer the best strength development. Any deviation from these values will negatively impact the strength development.

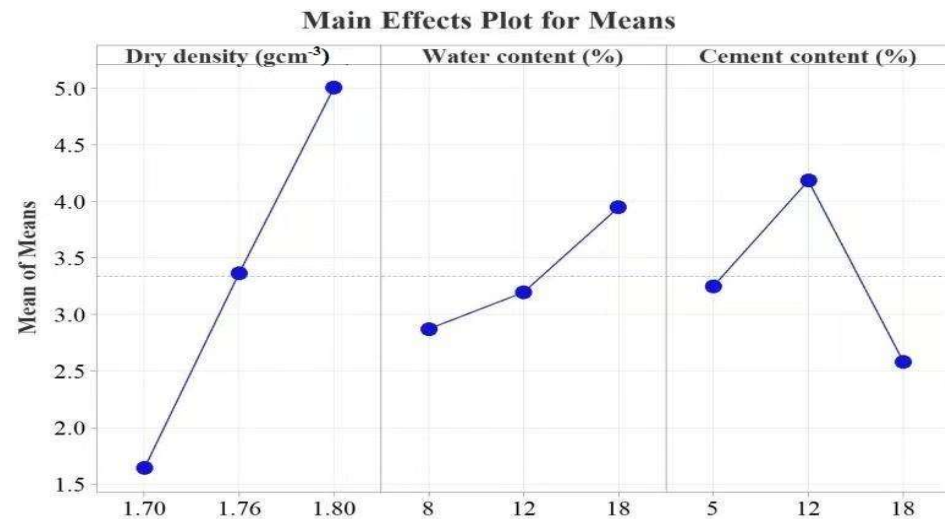


Figure 9. Effects of the control factors on USC.

#### 4.2. Grey Rational Analysis

Once calculations for GC and G were finished, their values were entered in Table 4. ANOVA was performed to assess the effects of the experimental input parameters on the GRA grade. The results of the ANOVA are presented in Table 5.  $\rho_d$ ,  $T$ ,  $w$ , and  $C$  influenced the GRA grade values with contributions of 79.09%, 10.30%, 3.94%, and 6.67%, respectively. A GRA near 1 in Table 4 can be considered a criterion that gives the best optimal conditions for  $K_{30}$ ,  $\rho$ , and  $UCS$ .

Table 4. Grey rational analysis.

ID	$K_{30}$	$\rho$	UCS	$K_{30}$	$\rho$	UCS	GRA G
	Normalized			Gray Relational Coefficient			
1	0.18	0.16	0.05	0.74	0.76	0.90	0.80
2	0.00	0.00	0.00	1.00	1.00	1.00	1.00
3	0.24	0.05	0.77	0.67	0.92	0.39	0.66
4	0.96	0.85	0.23	0.34	0.37	0.68	0.46
5	0.77	0.77	0.00	0.39	0.39	0.99	0.59
6	0.64	0.31	0.60	0.44	0.61	0.45	0.50
7	1.00	1.00	0.58	0.33	0.33	0.46	0.38
8	0.85	0.68	0.49	0.37	0.42	0.50	0.43
9	0.60	0.38	1.00	0.46	0.57	0.33	0.45

Table 5. ANOVA Analysis of GRA grade.

Factor	DF	Adss	Ad MS	F $\alpha = 0.5$	p Value	% Contribution
$\rho_d$	2	0.261	0.131	11.22	0.009	79.09
$w$	2	0.034	0.017	0.35	0.717	10.30
$C$	2	0.013	0.007	0.03	0.883	3.94
$T$	2	0.022	0.011	0.21	0.817	6.67
Error	-	-	-			
Total	8	0.33				100.00

#### 4.3. Regression Analysis

In this study, regression analyses were employed for modelling and predicting the response variables. Two different models were initially proposed: linear interactions and linear plus interactions. The best fitting models were selected. The highest performing predictive equations obtained from the analysis are given below. The equation reveals the nature of the relationships of the input parameters and their effect on the responses. Directly

proportional responses are acknowledged using a + sign, while the - sign represents the opposite. Equations (11)–(14) were identified as the best-performing equations for  $K_{30}$ ,  $\rho$ ,  $UCS$ , and  $GRA$ , respectively. The equations predicted the average  $K_{30}$ ,  $\rho$ ,  $UCS$ , and  $GRA$  with adjusted coefficients of correlation ( $R^2$ ) of 72.18%, 78.09%, 71.06%, and 55.63%, respectively. The individual unique predictor contributions for the equations are shown in Table 6.

$$K_{30} = 133.86 + 20.21\rho_d + 8.32T - 20.20\rho_d w + 2.0wC - 14.87w \tag{11}$$

$$P = 81.40 + 12.87\rho_d + 13.30T - 4.0\rho_d w + 20.23C - 11.30w \tag{12}$$

$$UCS = 3.34 + 1.21\rho_d - 0.95wC + 0.54w \tag{13}$$

$$GRA = 0.5749 - 0.203\rho_d + 0.0004wC + 0.0238wT - 0.0586CT + 0.0418\rho_d w \tag{14}$$

**Table 6.** Variance analysis of the regression equations.

Subgrade Reaction Modulus ( $K_{30}$ )						
Source	DF	Adj SS	Adj MS	F-Value	p-Value	% Contribution
Regression	5	6538.43	1307.69	5.15	0.104	89.57
$\rho_d$	1	1429.90	1429.90	5.63	0.098	19.59
$T$	1	242.29	242.29	0.95	0.401	3.32
$\rho_d w$	1	859.12	859.12	3.38	0.163	11.77
$wC$	1	8.03	8.03	0.03	0.870	0.11
$w$	1	1326.70	1326.70	5.23	0.106	18.17
Error	3	761.64	253.88			10.43
Total	8	7300.07				100.00
Soil electrical resistivity ( $\rho$ )						
Regression	5	6149.24	1229.85	5.90	0.087	90.77
$\rho_d$	1	994.34	994.34	4.77	0.117	14.68
$T$	1	424.27	424.27	2.04	0.249	6.26
$\rho_d w$	1	16.12	16.12	0.08	0.799	0.24
$C$	1	982.29	982.29	4.71	0.118	14.50
$w$	1	766.37	766.37	3.68	0.151	11.31
Error	3	625.02	208.34			9.23
Total	8	6774.26				100.00
Unconfined compressive strength ( $UCS$ )						
Regression	3	20.93	6.9778	7.55	0.03	81.89
$\rho_d$	1	5.47	5.4783	5.93	0.06	21.40
$wC$	1	2.24	2.2373	2.42	0.18	8.76
$w$	1	1.73	1.7281	1.87	0.23	6.77
Error	5	4.62	0.9245			18.08
Total	8	25.56				100.00
Grey rational analysis ( $GRA$ )						
Regression	5	0.225396	0.045079	3.01	0.197	83.36
$\rho_d$	1	0.108580	0.108580	7.24	0.074	40.16
$wC$	1	0.001064	0.001064	0.07	0.807	0.39
$wT$	1	0.000019	0.000019	0.00	0.974	0.01
$CT$	1	0.008024	0.008024	0.54	0.517	2.97
$T$	1	0.009048	0.009048	0.60	0.494	3.35
Error	3	0.044987	0.014996			16.64
Total	8	0.270383				100.00

#### 4.4. Implications for Practice

Several studies have suggested that  $K_{30}$  can reflect the strength, stiffness, and performance of compacted subgrade in China. However, we suggest that  $K_{30}$  is the main parameter that is commonly employed but is not the only parameter that can assure com-

pacted subgrade stiffness, performance, and deformation characteristics. Compacted soil typically remains in the elastic stage, away from the failure stage, as evidenced by the plate loading tests (refer to Figure 6b). As a result, using this indicator alone to capture the strength and stiffness characteristics is deemed ineffective. Additionally, the  $K_{30}$  test results are affected by factors such as  $w$ ,  $\rho_d$ ,  $T$ , and  $C$  (refer to Figure 7) for the cement-stabilized subgrade. The variability of  $w$ ,  $\rho_d$ , and  $C$  is reported to cause subgrade problems, such as swelling, subgrade cavity, and differential settlement.

There is no good indicator to reflect the changes in the physical and stiffness properties of the subgrade, particularly the  $K_{30}$ ,  $w$ ,  $T$ ,  $C$ , and  $\rho_d$  of the cement-stabilized subgrade for construction. However, practitioners are aware of how  $w$ ,  $T$ ,  $C$ , and  $\rho_d$  affect the test outcome of  $K_{30}$  and the performance of the compacted subgrade. Nonetheless, a qualitative method to instantaneously and concurrently assess the  $w$ ,  $T$ ,  $C$ , and  $\rho_d$  effects with  $K_{30}$  has always been associated with certain problems. Our test method solves this problem and serves as an advancement in compaction measurement systems and in situ testing technologies.

The proposed regression Equations (11)–(13) are presented to predict the average responses of  $K_{30}$ ,  $\rho$ , and UCS, which showed high performance with  $R^2$  values of 72.18%, 78.09%, and 71.06%, respectively. Use of the proposed equations is encouraged during the construction of cement-stabilized subgrade for similar soils utilized in this study with similar  $w$  and  $C$  requirements. Equation (14) was introduced as a unique equation that can give a combined unique identity to  $K_{30}$ , UCS, and  $\rho$ , considering the input factors employed in the study with an  $R^2$  of 55.63%. The test results presented in this study conclude that the proposed remediation was significant. Although our test method may be slow, its benefits outweigh those of commonly known methods in the literature.

## 5. Conclusions

A resistivity plate load device was developed to evaluate the properties of the cement-stabilized subgrade. Experimental studies were conducted on compacted cement soils according to the Taguchi orthogonal L9 array. Multivariate stepwise regression models were developed to predict  $K_{30}$ ,  $\rho$ , and UCS considering  $\rho_d$ ,  $T$ ,  $w$ , and  $C$  for compaction quality evaluation purposes. Our conclusions are as follows.

- (1) The resistivity plate load device can be efficiently used to assess the  $w$ ,  $C$ ,  $\rho_d$ , and  $T$  effects on  $K_{30}$  for the cement-stabilized subgrade for construction. Therefore, the device is recommended for field use. This recommendation must be evaluated and validated in the field with a vast variability in compacted soils with variable  $w$ ,  $C$ , and  $\rho_d$  properties that may confirm the implications of our laboratory observation.
- (2)  $K_{30}$  is significantly affected by  $C$ ,  $w$ ,  $\rho_d$ , and  $T$ . It is important within subgrade construction control protocols to confirm that compacted cement-stabilized subgrade  $C$ ,  $\rho_d$ ,  $T$ , and  $w$  are considered for a well-informed decision on  $K_{30}$ .
- (3) Different values of  $C$ ,  $\rho_d$ , and  $w$  have different effects on the USC, leading to variable USC strength values and confirming the need to control  $C$ ,  $\rho_d$ , and  $w$  during construction for enhanced performance.
- (4) The proposed regression models showed better performance, and therefore, are recommended to predict the average  $K_{30}$ ,  $\rho$ , UCS, and GRA grades during construction of the cement-stabilized subgrade for similar soils.

The statistical analysis presented in this study produced excellent results. The analysis should be treated as a simplified approach and a general guide that can be adopted for field compaction quality control for the cement-stabilized subgrade. Future studies include a field application of the test method and calibration of ICMVs for compaction management of the cement-stabilized subgrade. Notwithstanding, this study was a significant step towards providing a reliable reference for engineering practice in compaction quality control and a considerable step towards advancement in compaction measurement systems and in situ testing technologies.

**Author Contributions:** Conceptualization, H.F.; methodology, A.F.S.; validation, A.F.S. and H.F.; resources, H.W.; data curation, A.F.S.; writing—review and editing, H.F.; visualization, H.F.; supervision, H.F.; project administration, H.F.; funding acquisition, A.F.S.; investigation, A.F.S.; writing—original draft preparation, H.W.; Formal analysis and software, H.F. All authors have read and agreed to the published version of the manuscript.

**Funding:** This project was supported by the National Natural Science Foundation of China (51478279) and the Natural Science Foundation of Hebei Province (E2019210137).

**Institutional Review Board Statement:** Not applicable.

**Informed Consent Statement:** Not applicable.

**Data Availability Statement:** Data are available from the authors upon request.

**Acknowledgments:** The authors would like to acknowledge Gideon Blankson Abakah for presentation of experimental results and related discussions during departmental meetings.

**Conflicts of Interest:** The authors declare that they have no known competing financial interest or personal relationships that could have influenced the work reported in this paper.

## References

1. Jones, D.; Rahim, A.; Saadeh, S.; Harvey, J.T. *Guidelines for the Stabilization of Subgrade Soils in California*; State of California, Department of Transportation: Los Angeles, CA, USA, 2011.
2. Wei, X.; Ku, T. New Design Chart for Geotechnical Ground Improvement: Characterizing Cement-Stabilized Sand. *Acta Geotech.* **2020**, *15*, 999–1011. [[CrossRef](#)]
3. Bahar, R.; Benazzoug, M.; Kenai, S. Performance of Compacted Cement-Stabilised Soil. *Cem. Concr. Compos.* **2004**, *26*, 811–820. [[CrossRef](#)]
4. Little, D.N.; Nair, S. *Recommended Practice for Stabilization of Subgrade Soils and Base Materials*; National Academies of Sciences, Engineering, and Medicine: Washington, DC, USA, 2009.
5. Biswal, D.R.; Sahoo, U.C.; Dash, S.R. Non-Destructive Strength and Stiffness Evaluation of Cement-Stabilised Granular Lateritic Soils. *Road Mater. Pavement Des.* **2020**, *21*, 835–849. [[CrossRef](#)]
6. Fiedler, S.A.; Main, M.; DiMillio, A.F. In-Place Stiffness and Modulus Measurements. In *Performance Confirmation of Constructed Geotechnical Facilities*; ACSE: Reston, VA, USA, 2000; pp. 365–376. [[CrossRef](#)]
7. Commuri, S.; Zaman, M.M.; Arshadi, A.; Imran, S.; Barman, M. *Special Provisions for Intelligent Compaction of Stabilized Soil Subgrades*; Southern Plains Transportation Center: Norman, OK, USA, 2017.
8. Kumar, S.A.; Mazari, M.; Garibay, J.; AlDouri, R.E.; Nazarian, S.; Si, J. Compaction Quality Monitoring of Lime-Stabilized Clayey Subgrade Using Intelligent Compaction Technology. In Proceedings of the 2016 International Conference on Transportation and Development American Society of Civil Engineers, Houston, TX, USA, 26–29 June 2016. [[CrossRef](#)]
9. Nazarian, S.; Yuan, D.; Arellano, M. Quality Management of Base and Subgrade Materials with Seismic Methods. *Transp. Res. Rec.* **2002**, *1786*, 3–10. [[CrossRef](#)]
10. Barman, M.; Nazari, M.; Imran, S.A.; Commuri, S.; Zaman, M.; Beainy, F.; Singh, D. Quality Control of Subgrade Soil Using Intelligent Compaction. *Innov. Infrastruct. Solut.* **2016**, *1*, 23. [[CrossRef](#)]
11. Baaj, H. *Field and Lab Assessment for Cement-Stabilized Subgrade in Chatham, Ontario*; University of Waterloo: Waterloo, ON, Canada, 2018.
12. White, D.J.; Becker, P.; Vennapusa, P.K.; Dunn, M.J.; White, C.I. Assessing Soil Stiffness of Stabilized Pavement Foundations. *Transp. Res. Rec.* **2013**, *2335*, 99–109. [[CrossRef](#)]
13. Pongsivasathit, S.; Horpibulsuk, S.; Piyaphipat, S. Assessment of Mechanical Properties of Cement Stabilized Soils. *Case Stud. Constr. Mater.* **2019**, *11*, e00301. [[CrossRef](#)]
14. Tehrani, F.S.; Meehan, C.L. The Effect of Water Content on Light Weight Deflectometer Measurements. In *GeoFlorida 2010: Advances in Analysis, Modeling & Design*; ACSE: Reston, VA, USA, 2010; pp. 930–939. [[CrossRef](#)]
15. Hu, W.; Jia, X.; Zhu, X.; Su, A.; Du, Y.; Huang, B. Influence of Moisture Content on Intelligent Soil Compaction. *Autom. Constr.* **2020**, *113*, 103141. [[CrossRef](#)]
16. Kavussi, A.; Qorbaninik, M.; Hassani, A. The Influence of Moisture Content and Compaction Level on LWD Modulus of Unbound Granular Base Layers. *Transp. Geotech.* **2019**, *20*, 100252. [[CrossRef](#)]
17. Li, Y.; Zhang, Y.; Ceylan, H.; Kim, S. In Situ Evaluation of Using Lignosulfonate for Subgrade Stabilization. In Proceedings of the Geo-Congress 2020: Foundations, Soil Improvement, and Erosion, American Society of Civil Engineers, Reston, VA, USA, 25–28 February 2020; pp. 592–600. [[CrossRef](#)]
18. Liu, Y.; He, L.Q.; Jiang, Y.J.; Sun, M.M.; Chen, E.J.; Lee, F.-H. Effect of in Situ Water Content Variation on the Spatial Variation of Strength of Deep Cement-Mixed Clay. *Géotechnique* **2019**, *69*, 391–405. [[CrossRef](#)]
19. Xin, H.; Guo-jun, Z. Hardening Mechanism of Cement-Stabilized Soil. *Chin. J. Geotech. Eng.* **1994**, *1*, 62–68.

20. Walubita, L.F.; Mercado, V.; Lee, S.I.; Fuentes, L.; Villegas, J.M. Exploration of a Mechanistic Model for the Quantification of the Resilient Modulus Using Free-Free Resonant Column Testing. *Road Mater. Pavement Des.* **2021**, *22*, 2369–2383. [[CrossRef](#)]
21. Souliman, M.I.; GC, H.; Isied, M.M.; Walubita, L.F. Treated versus Untreated Aggregate Bases for Flexible Pavements: Nationwide Comparative Case Study. *Transp. Res. Rec.* **2020**, *2674*, 225–236. [[CrossRef](#)]
22. Shooshpasha, I.; Shirvani, R.A. Effect of Cement Stabilization on Geotechnical Properties of Sandy Soils. *Geomech. Eng.* **2015**, *8*, 17–31. [[CrossRef](#)]
23. Lazorenko, G.; Kasprzhitskii, A.; Khakiev, Z.; Yavna, V. Dynamic Behavior and Stability of Soil Foundation in Heavy Haul Railway Tracks: A Review. *Constr. Build. Mater.* **2019**, *205*, 111–136. [[CrossRef](#)]
24. Fu, Z.; Chen, S.; Han, H. Large-Scale Triaxial Experiments on the Static and Dynamic Behavior of an Artificially Cemented Gravel Material. *Eur. J. Environ. Civ. Eng.* **2020**, 1–21. [[CrossRef](#)]
25. Chae, Y.; Chiang, Y. Dynamic Behavior of Weak Soils Treated with Additives. In Proceedings of the 5th World Conference on Earthquake Engineering, Rome, Italy, 25–29 June 1973; pp. 1606–1610.
26. Walubita, L.F.; Lee, S.I.; Faruk, A.N.; Scullion, T.; Nazarian, S.; Abdallah, I. *Texas Flexible Pavements and Overlays: Year 5 Report-Complete Data Documentation*; Texas A&M Transportation Institute: College Station, TX, USA, 2017.
27. Ackah, F.S.; Zhuochen, N.; Huaiping, F. Effect of Wetting and Drying on the Resilient Modulus and Permanent Strain of a Sandy Clay by RLTT. *Int. J. Pavement Res. Technol.* **2021**, *14*, 366–377. [[CrossRef](#)]
28. Tannoury, G.A. Evaluation of Cement-Modified Soil (CMS) with Microcracking and Its Effects on Flexible Pavement Performance. Ph.D. Thesis, University of Kansas, Lawrence, KS, USA, 2019.
29. Kim, J.H.; Yoon, H.-K.; Lee, J.-S. Void Ratio Estimation of Soft Soils Using Electrical Resistivity Cone Probe. *J. Geotech. Geoenviron. Eng.* **2011**, *137*, 86–93. [[CrossRef](#)]
30. Choi, J.C.; Grande, L.; Park, J.; Mondol, N.H. Anisotropy Resistivity Measurement Using Modified Triaxial Cell: Estimation of Geometry Factor Using Numerical Simulation. In Proceedings of the 4th International Workshop on Rock Physics, Trondheim, Norway, 29 May–2 June 2017.
31. Naghibi, M.; Abuel-Naga, H.; Orense, R. Modified Odometer Cell to Measure Electrical Resistivity of Clays Undergoing Consolidation Process. *J. Test. Eval.* **2017**, *45*, 1261–1269. [[CrossRef](#)]
32. Zhang, D.; Chen, L.; Liu, S. Key Parameters Controlling Electrical Resistivity and Strength of Cement Treated Soils. *J. Cent. South Univ.* **2012**, *19*, 2991–2998. [[CrossRef](#)]
33. Tibbetts, C.M.; Watts, B.E.; Ferraro, C.C.; Huber, E.D. Improving the Utility of MIP Analysis for Cementitious Systems through Gaussian Process Regression Modeling to Predict Electrical Resistivity. *Cem. Concr. Compos.* **2021**, *116*, 103870. [[CrossRef](#)]
34. Côté, J.; Konrad, J.-M. A Generalized Thermal Conductivity Model for Soils and Construction Materials. *Can. Geotech. J.* **2005**, *42*, 443–458. [[CrossRef](#)]
35. Wang, Z.; Gelius, L.-J.; Kong, F.-N. Simultaneous Core Sample Measurements of Elastic Properties and Resistivity at Reservoir Conditions Employing a Modified Triaxial Cell—A Feasibility Study. *Geophys. Prospect.* **2009**, *57*, 1009–1026. [[CrossRef](#)]
36. Saydam, A.S.; Duckworth, K. Comparison of Some Electrode Arrays for Their IP and Apparent Resistivity Responses over a Sheet like Target. *Geoexploration* **1978**, *16*, 267–289. [[CrossRef](#)]
37. Dahlin, T.; Zhou, B. A Numerical Comparison of 2D Resistivity Imaging with 10 Electrode Arrays. *Geophys. Prospect.* **2004**, *52*, 379–398. [[CrossRef](#)]
38. Zhou, Z.; Yang, H.; Wan, Z.H.; Liu, B.C. Computational Model for Electrical Resistivity of Soil–Rock Mixtures. *J. Mater. Civ. Eng.* **2016**, *28*, 06016009. [[CrossRef](#)]
39. Fortier, R.; Allard, M.; Seguin, M.-K. Effect of Physical Properties of Frozen Ground on Electrical Resistivity Logging. *Cold Reg. Sci. Technol.* **1994**, *22*, 361–384. [[CrossRef](#)]
40. Hong, C.-H.; Chong, S.-H.; Cho, G.-C. Theoretical Study on Geometries of Electrodes in Laboratory Electrical Resistivity Measurement. *Appl. Sci.* **2019**, *9*, 4167. [[CrossRef](#)]
41. Horpibulsuk, S.; Katkan, W.; Sirilerdwattana, W.; Rachan, R. Strength Development in Cement Stabilized Low Plasticity and Coarse Grained Soils: Laboratory and Field Study. *Soils Found.* **2006**, *46*, 351–366. [[CrossRef](#)]
42. Jeyapaul, R.; Shahabudeen, P.; Krishnaiah, K. Quality Management Research by Considering Multi-Response Problems in the Taguchi Method—A Review. *Int. J. Adv. Manuf. Technol.* **2005**, *26*, 1331–1337. [[CrossRef](#)]
43. Sevinc, A.H.; Durgun, M.Y.; Eken, M. A Taguchi Approach for Investigating the Engineering Properties of Concretes Incorporating Barite, Colemanite, Basaltic Pumice and Ground Blast Furnace Slag. *Constr. Build. Mater.* **2017**, *135*, 343–351. [[CrossRef](#)]
44. Ho, T.-O.; Chen, W.-B.; Yin, J.-H.; Wu, P.-C.; Tsang, D.C. Stress-Strain Behaviour of Cement-Stabilized Hong Kong Marine Deposits. *Constr. Build. Mater.* **2021**, *274*, 122103. [[CrossRef](#)]
45. Jin, L.; Song, W.; Shu, X.; Huang, B. Use of Water Reducer to Enhance the Mechanical and Durability Properties of Cement-Treated Soil. *Constr. Build. Mater.* **2018**, *159*, 690–694. [[CrossRef](#)]
46. Slebi-Acevedo, C.J.; Silva-Rojas, I.M.; Lastra-Gonzalez, P.; Pascual-Munoz, P.; Castro-Fresno, D. Multiple-Response Optimization of Open Graded Friction Course Reinforced with Fibers through CRITIC-WASPAS Based on Taguchi Methodology. *Constr. Build. Mater.* **2020**, *233*, 117274. [[CrossRef](#)]
47. Besson, A.; Cousin, I.; Dorigny, A.; Dabas, M.; King, D. The Temperature Correction for the Electrical Resistivity Measurements in Undisturbed Soil Samples: Analysis of the Existing Conversion Models and Proposal of a New Model. *Soil Sci.* **2008**, *173*, 707–720. [[CrossRef](#)]

48. Wang, D.; Zentar, R.; Abriak, N.E. Temperature-Accelerated Strength Development in Stabilized Marine Soils as Road Construction Materials. *J. Mater. Civ. Eng.* **2017**, *29*, 04016281. [[CrossRef](#)]
49. Tabbagh, J.; Samouëlian, A.; Tabbagh, A.; Cousin, I. Numerical Modelling of Direct Current Electrical Resistivity for the Characterisation of Cracks in Soils. *J. Appl. Geophys.* **2007**, *62*, 313–323. [[CrossRef](#)]
50. White, D.J.; Harrington, D.; Thomas, Z. Fly Ash Soil Stabilization for Non-Uniform Subgrade Soils. In *IHRB Project TR-461, FHWA Project*; Iowa State University: Ames, IA, USA, 2005; Volume 4.
51. Sariosseiri, F.; Muhunthan, B. Effect of Cement Treatment on Geotechnical Properties of Some Washington State Soils. *Eng. Geol.* **2009**, *104*, 119–125. [[CrossRef](#)]
52. Guthrie, W.S.; Michener, J.E.; Wilson, B.T.; Eggett, D.L. Effects of Environmental Factors on Construction of Soil–Cement Pavement Layers. *Transp. Res. Rec.* **2009**, *2104*, 71–79. [[CrossRef](#)]
53. Chai, M.; Zhang, H.; Zhang, J.; Zhang, Z. Effect of Cement Additives on Unconfined Compressive Strength of Warm and Ice-Rich Frozen Soil. *Constr. Build. Mater.* **2017**, *149*, 861–868. [[CrossRef](#)]
54. Little, D.N.; Males, E.H.; Prusinski, J.R.; Stewart, B. Cementitious Stabilization. In *Transportation in the New Millennium*; National Academies of Sciences, Engineering, and Medicine: Washington, DC, USA, 2000.
55. Ikhlef, N.S.; Ghembaza, M.S.; Dadouch, M. Effect of Cement and Compaction on the Physicochemical Behavior of a Material in the Region of Sidi Bel Abbes. *Eng. Technol. Appl. Sci. Res.* **2014**, *4*, 677–680. [[CrossRef](#)]
56. Cho, G.-C.; Dodds, J.; Santamarina, J.C. Particle Shape Effects on Packing Density, Stiffness, and Strength: Natural and Crushed Sands. *J. Geotech. Geoenviron. Eng.* **2006**, *132*, 591–602. [[CrossRef](#)]
57. Tatsuoka, F.; Hashimoto, T.; Tateyama, K. Soil Stiffness as a Function of Dry Density and the Degree of Saturation for Compaction Control. *Soils Found.* **2021**, *61*, 989–1002. [[CrossRef](#)]
58. Chen, L.; Liu, S.Y.; Du, Y.J.; Jin, F. Unconfined Compressive Strength Properties of Cement Solidified/Stabilized Lead-Contaminated Soils. *Yantu Gongcheng Xuebao/Chin. J. Geotech. Eng.* **2010**, *32*, 1898–1903. [[CrossRef](#)]
59. Ajmera, B.; Tiwari, B.; Koirala, J.; Obaid, Z. Compaction Characteristics, Unconfined Compressive Strengths, and Coefficients of Permeability of Fine-Grained Soils Mixed with Crumb-Rubber Tire. *J. Mater. Civ. Eng.* **2017**, *29*, 04017148. [[CrossRef](#)]
60. Parreira, A.B.; Kobayashi, A.R.K.; Silvestre, O.B., Jr. Influence of Portland Cement Type on Unconfined Compressive Strength and Linear Expansion of Cement-Stabilized Phosphogypsum. *J. Environ. Eng.* **2003**, *129*, 956–960. [[CrossRef](#)]
61. Ribeiro, D.; Néri, R.; Cardoso, R. Influence of Water Content in the UCS of Soil-Cement Mixtures for Different Cement Dosages. *Procedia Eng.* **2016**, *143*, 59–66. [[CrossRef](#)]
62. Azadegan, O.; Jafari, S.H.; Li, J. Compaction Characteristics and Mechanical Properties of Lime/Cement Treated Granular Soils. *Electron. J. Geotech. Eng.* **2012**, *17*, 2275–2284.
63. Horpibulsuk, S.; Rachan, R.; Chinkulkijniwat, A.; Raksachon, Y.; Suddeepong, A. Analysis of Strength Development in Cement-Stabilized Silty Clay from Microstructural Considerations. *Constr. Build. Mater.* **2010**, *24*, 2011–2021. [[CrossRef](#)]